POLYPUBLIE

Optical modeling of internal and external in-plane Fabry–Pérot interferometers for sensing polymer swelling

Régis Guertin, Ali Khurshidi, Suhas Kottigegollahalli Sreenivas, Yves-Alain Peter

Document en libre accès dans PolyPublie
Open Access document in PolyPublie

Date	2026
Type	Article de revue / Article
Version	Version finale avant publication / Accepted version
URL de PolyPublie PolyPublie URL	https://publications.polymtl.ca/82336/
Évaluation par les pairs Peer reviewed	Révisé par les pairs / Refereed
Conditions d'utilisation Terms of use	© Tous droits réservés / All rights reserved
Référence Citation	Guertin, R., Khurshidi, A., Kottigegollahalli Sreenivas, S., & Peter, Y.-A. (2026). Optical modeling of internal and external in-plane Fabry–Pérot interferometers for sensing polymer swelling. Journal of Optical Microsystems, 6(3), 033501 (9 pages). https://doi.org/10.1117/1.jom.6.3.033501

Publication officielle
Official publication

Titre de la revue Journal title	Journal of Optical Microsystems (vol. 6, no. 3)
Maison d'édition Publisher	SPIE - International Society for Optical Engineering
URL officielle Official URL	https://doi.org/10.1117/1.jom.6.3.033501
Mention légale Legal notice	2026 Society of Photo-Optical Instrumentation Engineers (SPIE). One print or electronic copy may be made for personal use only. Systematic reproduction and distribution, duplication of any material in this publication for a fee or for commercial purposes, and modification of the contents of the publication are prohibited.

Ce fichier a été téléchargé à partir de PolyPublie, le dépôt institutionnel de Polytechnique Montréal
This file has been downloaded from PolyPublie, the institutional repository of Polytechnique Montréal
https://publications.polymtl.ca

Optical Modeling of Internal and External In-Plane Fabry-Perot Interferometers for Sensing Polymer Swelling

Régis Guertin[a,*], **Ali Khurshidi**[a], **Marc-Antoine Bianki**[a], **Suhas Kottigegollahalli-Sreenivas**[a,b], **Yves-Alain Peter**[a]
[a]Polytechnique Montréal, Department of Engineering Physics
[b]Birla Institute of Technology and Science, Department of Electrical and Electronics Engineering

Abstract. This paper presents an optical model for polymer-functionalized in-plane Fabry-Perot Interferometers (FPIs), developed to enhance device sensitivity by exploiting polymer swelling as a micro-actuation mechanism for environmental and gas sensing applications. We investigate both internal and external optical cavity designs and fabricate external FPIs on silicon with adjustable cavity lengths. In the external configuration, the polymer interaction length is decoupled from the optical cavity length, allowing polymer swelling to be efficiently transduced into a change in resonant wavelength. This work is validated by using temperature modulation to induce polymer swelling. The external configuration enables an increase in sensitivity by a factor of two and the measurement of polymers opaque to infrared light, broadening material options for future applications.

Keywords: Fabry-Perot, Silicon (110), External Cavity, Polymer Actuator, Micro-mirrors, Anisotropic Etching.

*Régis Guertin, regis.guertin@etud.polymtl.ca

1 Introduction

Polymer swelling is widely used to measure environmental parameters such as temperature, gas concentration, and humidity.[1–6] Temperature-induced swelling originates from thermal expansion governed by the linear coefficient of thermal expansion (CTE), while gas and humidity induce swelling through absorption and chemical interactions with the polymer.[7] In all cases, polymer swelling can be interpreted as a micro-actuation mechanism capable of producing controlled mechanical deformations, which can be efficiently transduced using optical resonators. This principle has been integrated into a variety of photonic platforms, such as optical fibers,[8–10] microdisks,[4,5] and in-plane FPIs.[11,12]

Microdisk resonators provide higher optical quality factors (Q-factors) than FPIs and non-resonant interferometers, making them particularly well suited for achieving low limits of detection

(LOD).[13] However, their operation often relies on suspended geometries,[4,5] complicating large-scale integration and multiplexed sensing with wide variety of polymers. In contrast, in-plane FPIs fabricated through silicon micromachining present a robust and scalable alternative.[12,14,15] These devices can be encapsulated, arranged in sensor arrays, and individually functionalized with various polymers during a final fabrication step. The functionalisation is versatile as any liquid-state polymer can be deposited directly into the cavity, including melts, solutions, and in-situ polymerization. The sensing mechanism relies on shifts in the resonance wavelength, which arises from polymer swelling in the presence of external stimuli. The stimuli changes both the polymer's refractive index and polymer's microchannel length by mirror deformation, modulating the optical response.

To improve the performance of in-plane FPIs, previous studies have pursued two main approaches. One involves increasing the Q-factor by fabricating curved mirrors using deep reactive ion etching,[16] while others employ anisotropic etching to define planar mirrors with reduced surface roughness.[17] Although these techniques enhance the Q-factor and generally lower the limit of detection,[13] they do not affect the device's intrinsic sensitivity. Sensitivity therefore remains a key limitation and must be addressed through the combined engineering of both the polymer actuator and the optical cavity configuration.

External optical cavity architectures have been proposed as a means to enhance sensitivity by modifying the relationship between mechanical deformation and optical response.[18] However, such concepts have not yet been implemented in an on-chip, in-plane configuration compatible with silicon micromachining.

In this work, we develop an optical model for polymer-functionalized in-plane FPIs that exploits polymer swelling as a micro-actuation mechanism. Both internal and external cavity con-

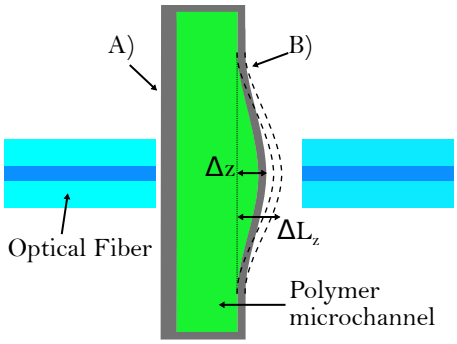


Fig 1 Swelling model of a polymer in a microchannel channel. The dotted line represents the cavity at rest and the dashed line is the swelling without constrains. A) Rigid and B) Flexible mirrors

figurations are investigated, and external FPIs with adjustable optical cavity lengths are fabricated on silicon. By decoupling the polymer interaction length from the optical cavity length, polymer swelling is efficiently transduced into a change in cavity size. Experimental validation is performed by inducing polymer swelling through temperature modulation, which serves as a controlled stimulus to emulate swelling responses expected from various external perturbations.

2 Optical Model

The device consists of a polymer confined within a microchannel etched in silicon and formed with flexible and rigid walls as illustrated in Fig 1. Upon external stimuli, the polymer swells and exerts pressure on the flexible wall causing a deformation, thus increasing the length of the microchannel by Δz. To model this deformation, the normalized swelling of the polymer under stimuli in a polymer cavity of length L is expressed as follows:

$$\frac{\Delta z}{L} = R\alpha\Delta T, \tag{1}$$

where α is the CTE and ΔT the change in temperature. The mechanical factor R accounts for mirror stiffness and confinement between rigid plates.[19]

To measure this displacement, a FPI is used. Its wavelength peaks correspond to the resonance condition which is function of the optical cavity length (d) and the refractive index (n) and is expressed as

$$m\lambda = 2nd, \tag{2}$$

where m is the resonance order and λ the wavelength. From this resonance condition, the resulting normalized wavelength shift ($\Delta\lambda$) can be determined with:

$$\frac{\Delta\lambda}{\lambda} = \frac{\Delta d}{d} + \frac{\Delta n}{n} + \frac{\Delta n \Delta d}{nd}. \tag{3}$$

In this study, the variation of the refractive index of the polymer is considered small compared to mechanical swelling based on previous results.[14] In particular, St-Gelais *et al.* reported that the contribution from mechanical expansion is at least one order of magnitude larger than that from refractive index changes, justifying to neglect the refractive index variations and associated higher-order terms. Considering the mechanical displacement, two distinct configurations can be studied depending on the position of the optical cavity and the polymer's microchannel, as illustrated in Fig 2. In Fig 2a, the internal configuration, the optical cavity is located in between two gold coated silicon mirrors and within the polymer microchannel. In Fig 2b, the external configuration, the optical cavity is located in between a reflective gold coated optical fiber tip and a gold coated silicon mirror.

In the internal configuration, the polymer is located within the optical cavity, making the optical cavity and the polymer microchannel coupled together and equal in length ($d = L$). Thus, the

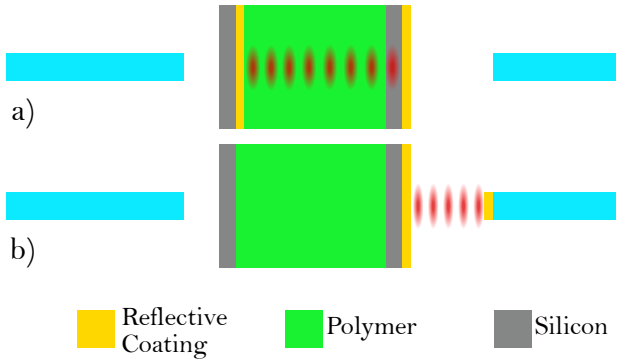


Fig 2 Optical device schematics and location of resonances in red. a) Internal configuration where the optical cavity is located in the polymer's microchannel. b) External configuration where the optical cavity is located outside the polymer's microchannel.

microchannel's change in length is directly equal to the cavity's mirror displacement (Δz=Δd) and the wavelength shift is expressed as

$$\frac{\Delta\lambda}{\lambda} = R\alpha\Delta T. \tag{4}$$

The sensitivity (S) of the device is defined as the ratio of the wavelength shift to the magnitude of the stimuli and is expressed as

$$\frac{S}{\lambda} = R\alpha. \tag{5}$$

This configuration's sensitivity doesn't depend on the optical cavity's characteristics but only on the polymer's swelling characteristics and the mechanical factor.

In the external configuration, the optical cavity length is decoupled from the polymer's length. In this case, the change in the cavity length is still equal to the change of the microchannel's length

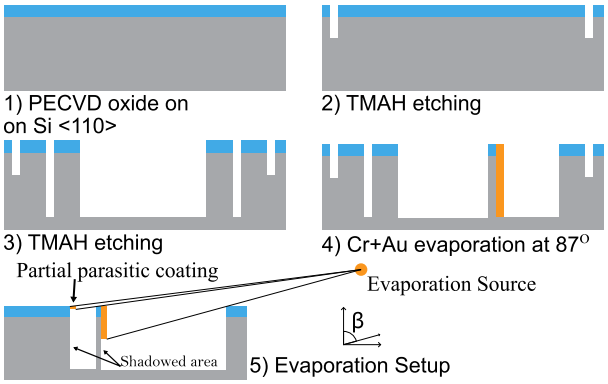


Fig 3 1)-4)Fabrication Process. 5) Evaporation setup with evaporation angle β and target metal to evaporate at the source.

but in the opposite direction ($\Delta d = -\Delta z$). Thus, the sensitivity of the device is expressed as:

$$\frac{S}{\lambda} = -R\alpha\frac{L}{d}. \tag{6}$$

In the external configuration, the optical factor $\frac{L}{d}$ modulates the sensitivity by decoupling the polymer channel's length from the optical cavity length. Reducing the FPI's optical length (d) increases the wavelength shift for an equivalent mirror displacement, and thus the sensitivity. From an optical perspective, a shorter cavity also increases the free spectral range (FSR), often yielding fewer resonance peak within the scanning range while having no effect on the dynamic range. Additionally, according to Eq. (6), a longer polymer microchannel should produce greater swelling along the optical axis, enhancing response compared with the internal design. However, the effect of the mechanical factor and cavity length RL remains unclear, and increasing L does not guarantee higher sensitivity as it is influenced by the geometry and mechanical properties.[19]

3 Fabrication and Optical Characterization

Devices for external configuration were fabricated on silicon (110) wafers using anisotropic etching with TMAH as shown in Fig 3 using a similar process as presented in previous work.[17] A

$250\,\mathrm{nm}$ SiO_2 layer was deposited by PECVD at $300\,^{\circ}\mathrm{C}$ to reduce surface roughness during etching.[20] The wafer orientation was aligned within 0.05° of the [112] direction with a TMAH first etch. The device pattern was subsequently etched again to achieve a depth of $100\,\mu\mathrm{m}$. In the external configuration, a reflective coating consisting of $8\,\mathrm{nm}$ of chromium and $22\,\mathrm{nm}$ of gold was evaporated at an angle of 87°, selectively coating only the exterior of one mirror per polymer channel, as seen in Fig 2b. This contrast with the internal configuration where the coating was applied in a more symmetrical manner with an evaporation angle of 35°.[12,17] The angled deposition results in a partial coating of about $3\,\mu\mathrm{m}$ on top of the second silicon wall, which may cause unwanted reflections if within the optical path. Thus, alignment must be precise to avoid parasitic cavities. The etching depth mitigates this effect, as each fiber with a radius of $62.5\,\mu\mathrm{m}$, had its core positioned below the parasitic reflective area. In the external configuration, the second mirror is formed by a cleaved optical fiber coated with the same reflective coating. The device functionalisation was performed by injecting liquid-phase polymers into the microchannels through capillary forces. Twelve devices were fabricated, of which half were functionalized with in-situ polymerized PDMS and the other half with in-situ UV cured SU-8 2000.

For the optical characterization, a tunable laser source (Keysight N7776C) ranging from $1450\,\mathrm{nm}$ to $1650\,\mathrm{nm}$ and photodiodes (Keysight N7745C) are used. Light was coupled to the cavities using cleaved SMF-28 optical fibers. All fibers were positioned at various distances from the reflecting mirrors to adjust the optical cavity length and were fixed using UV curable adhesive. Optical spectra are shown in Fig 4. The optical cavity length d is calculated from the interference peaks

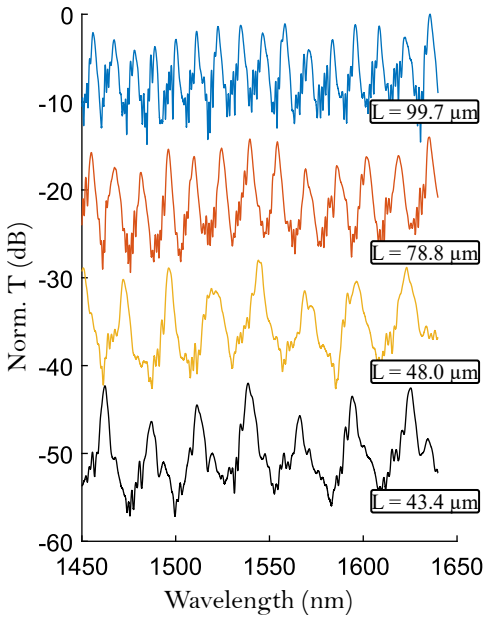


Fig 4 Optical spectra in external configuration for different cavity length with an empty polymer channel.

using

$$d = \frac{1}{2n_a} \frac{\lambda_2 \lambda_1}{\lambda_2 - \lambda_1} \tag{7}$$

where λ_1 and λ_2 are two adjacent resonant peak wavelengths and n_a the refractive index of air. From Fig 4, the Q-factor ranges from 250 to 500, lower than those in prior devices being on the order of 2×10^3.[17] This reduction is due to the imperfect alignments of the optical fiber, which lacks the inherent parallelism of etched (111) silicon mirrors , increasing the limit of detection by a factor 4 to 8[13]. In addition, parasitic cavities appear, caused by either reflections from non-coated silicon walls or higher-order modes induced by fiber misalignment.

4 Results and discussion

The sensitivities to temperature were measured by tracking the resonant peak wavelength of the devices as the temperature varied. A Thorlabs MTD1020 Peltier controller was used to control

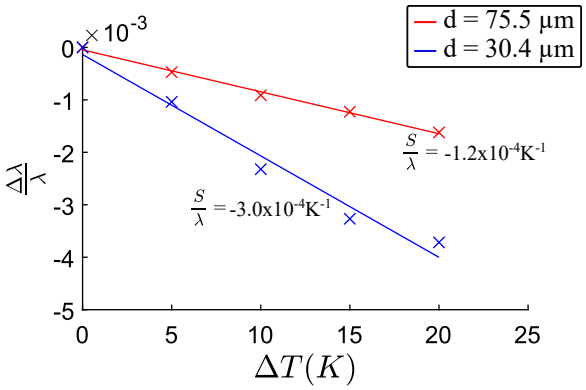


Fig 5 Wavelength shift as a function of temperature change for two PDMS filled cavities. The reference temperature is 15 °C.

the temperature from 15 °C to 35 °C with a maximum deviation of 10 mK. Fabricated samples had polymer microchannels length of 63 µm and optical cavities ranging from 30 µm to 255 µm. Figure 5 shows the response of two of the six PDMS-filled cavities with different optical cavity length. The six other cavities filled with SU-8 were tested under the same conditions and yielded similar results. The model in Eq. (4) is fitted and the slope corresponds to the sensitivity. Both polymers showed a linear response, in contrast with earlier reports of non-linear effects caused by phase transitions.[11] The figure demonstrates that the sensitivity varies with optical cavity length. According to Eq. (3), a mechanical displacement on the order of 75 nm corresponds to normalized wavelength shifts of 1×10^{-3} for a 75.5 µm optical cavity and 2.5×10^{-3} for a 30.4 µm optical cavity. Figure 6 shows the measured sensitivity as a function of inverse cavity length. The model in Eq. (6) is fitted to the experimental results for both polymers. By calculating the slope, the $R\alpha L$ coefficients are evaluated to 6.1×10^{-9} m K^{-1} for PDMS and 1.5×10^{-8} m K^{-1} for SU-8. As both polymer microchannels are 63 µm in length, the $R\alpha$ coefficients are evaluated to 0.96×10^{-4} K^{-1} and 2.37×10^{-4} K^{-1} respectively. These values contrast with reported CTE of 2.50×10^{-4} K^{-1} for PDMS[21] and 1.50×10^{-4} K^{-1} for SU-8.[22] These differences likely reflect mechanical effects with $R \neq 1$. The thickness of the mirror might play a role as the PDMS sensors, which had

thicker mirrors, showed lower sensitivity. Non-flexible mirrors have previously been found to reduce polymer swelling sensor sensitivity.[14] It is worth noting that, according to Timoshenko *et al.*, the stiffness of a plate scales with the cube of its thickness,[23] which may contribute to this behavior, although a more detailed analysis would be required to confirm this effect in the present configuration.[24] Moreover, variations in deposition technique cause large differences in reported CTEs,[25] moreover contributing to the discrepancy. To further increase the sensitivity, $R\alpha$ should nonetheless be increased and more work has to be done to clearly identify the underlying mechanics. Variation in sensitivity, seen as deviations from the model, may also arise due to fabrication deviations such as uneven polymer filling, mirror thickness variation, and inconsistent fiber positioning. Since the mirror is fixed on three sides, the deformation is uneven, making fiber positioning critical. The current setup may not achieve optimal placement.

The internal cavity model predicts the sensitivity being directly proportional to $R\alpha$. For the PDMS external devices, the maximum sensitivity obtained is $1.93 \times 10^{-4}\,\mathrm{K}^{-1}$, which is twice larger than $R\alpha$. For the SU-8 external sensors, the maximum sensitivity obtained is $3.89 \times 10^{-4}\,\mathrm{K}^{-1}$ which is 1.6 times larger than $R\alpha$. These results show that decoupling the polymer microchannel

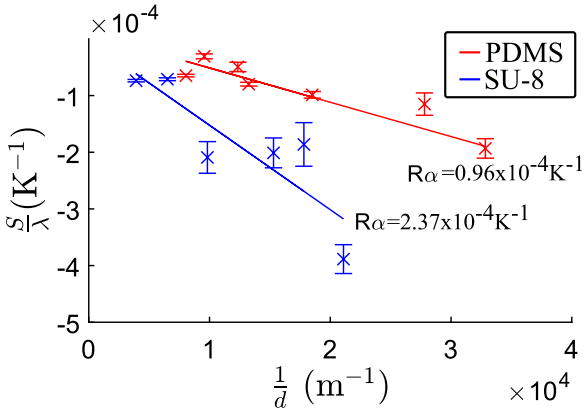


Fig 6 Normalized temperature sensitivity of SU-8 and PDMS functionalized sensors as a function of the inverse optical cavity length, from 30 µm to 255 µm. The mirror thickness of PDMS and SU-8 sensors are 3.7 µm and 2.7 µm respectively. The polymer microchannel is 63 µm long for all devices.

to the optical cavity by having external cavities is an avenue to increase the sensitivity. However, internal cavities remain pertinent when variation in refractive index dominates swelling, which is unexplored in this work. Even greater sensitivity could be achieved with smaller external optical cavities. However, positioning the fiber's mirror parallel to the chip's mirror remains manually challenging. This step limits the minimum cavity length to about $30\,\mu\mathrm{m}$, as shorter optical cavities could not be fabricated due to losses of the resonances. Integrating the mirror directly on the chip would ease alignment and allow for shorter cavities, but it would require major changes to the fabrication process. One possible process would fabricate the mirrors, evaporate a metal coating, and etch the polymer channel afterwards. Other methods reported in the literature may help to increase alignment tolerances. A microsphere placed inside the cavity was previously reported raising the Q factor and reducing misalignment sensitivity up to 2° for cavities as short as $4\,\mu\mathrm{m}$.[26] Alternatively, etching a concave mirror at the fiber tip using a CO_2 laser has allowed other groups to fabricate cavities as small as $3\,\mu\mathrm{m}$[27] and $10\,\mu\mathrm{m}$,[28] which would yield an order of magnitude increase in sensitivity compared to the fabricated devices of this work.

5 Conclusion

We developed a probing scheme that efficiently transduces polymer swelling into optical wavelength shifts using external FPIs cavities. An optical model linking polymer swelling, microchannel length, and optical cavity length was established for both internal and external configurations. The model predicts higher and tunable sensitivity for external FPIs through decoupling of the polymer interaction length from the optical cavity length. Twelve external FPIs with adjustable cavity lengths were fabricated and functionalized to validate this approach. Polymer swelling was emulated via temperature modulation, and experimental results confirmed that shorter optical cavities

yield increased sensitivity, achieving up to a twofold improvement over internal FPIs. This configuration enables extraction of the combined parameter $R\alpha$, while independent determination of these quantities requires additional methods.

Placing the resonator outside the polymer channel further extends the design's versatility, as it allows the measurement of polymers opaque to infrared light. This flexibility opens the door to broader material choices and new applications, including gas sensing and environmental monitoring. Looking ahead, integrating the external cavity directly on chip with a polymer channel in silicon (110) would mitigate Q-factor loss from fiber misalignment, simplify alignment, and improve overall detection performance.

Disclosures

The authors declare that there are no financial interests, commercial affiliations, or other potential conflicts of interest that could have influenced the objectivity of this research or the writing of this paper.

Code and Data Availability

All data in support of the findings of this paper are available within the article.

Acknowledgments

The authors would like to thank the Microfabrication Laboratory at Polytechnique Montreal as well as the Laboratory of Micro and Nanofabrication at INRS for the assistance with the microfabrication process. This work was supported in part by the Canadian Microelectronics Corporation (CMC), the Natural Sciences and Engineering Research Council of Canada (NSERC) [ALLRP

577113–2022, RGPIN-2020-06692]. The authors acknowledge the use of AI tools for linguistic refinement, however, the final content was reviewed and edited by the authors, who take full responsibility for the integrity of the work.

References

1 F. Zee and J. W. Judy, "Micromachined polymer-based chemical gas sensor array," *Sensors and Actuators B: Chemical* **72**(2), 120–128 (2001). [doi.org/10.1016/S0925-4005(00)00638-9].

2 J. Feller and Y. Grohens, "Evolution of electrical properties of some conductive polymer composite textiles with organic solvent vapours diffusion," *Sensors and Actuators B: Chemical* **97**, 231–242 (2004). [doi.org/10.1016/j.snb.2003.08.021].

3 D. Fu, J. Chung, Q. Liu, *et al.*, "Polymer coated silicon microring device for the detection of sub-ppm volatile organic compounds," *Sensors and Actuators B: Chemical* **257**, 136–142 (2018). [doi.org/10.1016/j.snb.2017.10.166].

4 M.-A. Bianki, R. Guertin, C. Lemieux-Leduc, *et al.*, "Suspended whispering gallery mode resonators made of different polymers and fabricated using drop-on-demand inkjet printing for gas sensing applications," *Sensors and Actuators B: Chemical* **420**, 136460 (2024). [doi.org/10.1016/j.snb.2024.136460].

5 C. Lemieux-Leduc, R. Guertin, M.-A. Bianki, *et al.*, "All-polymer whispering gallery mode resonators for gas sensing," *Optics express* **29**(6), 8685–8697 (2021). [doi.org/10.1364/OE.417703].

6 T. Yeo, T. Sun, K. Grattan, *et al.*, "Characterisation of a polymer-coated fibre Bragg grating

sensor for relative humidity sensing," *Sensors and Actuators B: Chemical* **110**(1), 148–156 (2005). [doi.org/10.1016/j.snb.2005.01.033].

7 M. Belmares, M. Blanco, W. A. Goddard III, *et al.*, "Hildebrand and hansen solubility parameters from molecular dynamics with applications to electronic nose polymer sensors," *Journal of computational chemistry* **25**(15), 1814–1826 (2004). [doi.org/10.1002/jcc.20098].

8 D. Yi, F. Liu, Y. Geng, *et al.*, "High-sensitivity and large-range fiber optic temperature sensor based on PDMS-coated Mach-Zehnder interferometer combined with FBG," *Optics express* **29**(12), 18624–18633 (2021). [doi.org/10.1364/OE.428384].

9 Y. Zhu, Y. Zhang, Q. Tang, *et al.*, "Double-cavity Fabry-Perot interferometer sensor based on polymer-filled hollow core fiber for simultaneous measurement of temperature and gas pressure," *Sensors* **25**(8), 2396 (2025). [doi.org/10.3390/s25082396].

10 Q. Liu, Y. Zhan, S. Zhang, *et al.*, ""optical tentacle" of suspended polymer micro-rings on a multicore fiber facet for vapor sensing," *Optics Express* **28**(8), 11730–11741 (2020). [doi.org/10.1364/OE.390145].

11 R. Guertin, M.-A. Bianki, and Y.-A. Peter, "Low-cost fabrication of an on-chip Fabry-Perot interferometer for dry environmental monitoring," in *2023 International Conference on Optical MEMS and Nanophotonics (OMN) and SBFoton International Optics and Photonics Conference (SBFoton IOPC)*, 1–2, IEEE (2023). [doi.org/10.1109/OMN/SBFotonIOPC58971.2023.10230951].

12 R. Guertin, M.-A. Bianki, O. Figueroa, *et al.*, "Polymer-functionalized on-chip Fabry-Perot interferometer for CO_2 and CH_4 sensing," in *2024 International*

Conference on Optical MEMS and Nanophotonics (OMN), 1–2, IEEE (2024). [doi.org/10.1109/OMN61224.2024.10685237].

13 I. M. White and X. Fan, "On the performance quantification of resonant refractive index sensors," *Optics express* **16**(2), 1020–1028 (2008). [doi.org/10.1364/OE.16.001020].

14 R. St-Gelais, G. Mackey, J. Saunders, *et al.*, "Gas sensing using polymer-functionalized deformable Fabry-Perot interferometers," *Sensors and Actuators B: Chemical* **182**, 45–52 (2013). [doi.org/10.1016/j.snb.2013.02.016].

15 R. Guertin, M.-A. Bianki, C. Lemieux-Leduc, *et al.*, "Multi-gas detection using Fabry-Perot interferometers on silicon chip," *Sensors and Actuators B: Chemical* **335**, 129655 (2021). [doi.org/10.1016/j.snb.2021.129655].

16 N. Gaber, Y. M. Sabry, M. Erfan, *et al.*, "High-Q Fabry–Pérot micro-cavities for high-sensitivity volume refractometry," *Micromachines* **9**(2), 54 (2018). [doi.org/10.3390/mi9020054].

17 R. Guertin, T. Lacasse, C. Lemieux-Leduc, *et al.*, "High-performance, low-cost on-chip Fabry-Perot interferometer with microfluidic channel using single anisotropic wet etching," *Journal of Microelectromechanical Systems* **32**(4), 347–351 (2023). [doi.org/10.1109/JMEMS.2023.3278451].

18 C. Zhu, H. Zheng, L. Ma, *et al.*, "Advances in fiber-optic extrinsic Fabry-Perot interferometric physical and mechanical sensors: A review," *IEEE Sensors Journal* **23**(7), 6406–6426 (2023). [doi.org/10.1109/JSEN.2023.3244820].

19 G.-K. Lau, J. F. Goosen, and F. van Keulen, "Thermo-elastic behavior of a polymeric layer

bonded between rigid interfaces," *International Journal of Solids and Structures* **45**(18-19), 5152–5164 (2008). [doi.org/10.1016/j.ijsolstr.2008.05.016].

20 L. Sène, R. Guertin, and Y.-A. Peter, "Optimization of Fabry-Perot interferometer performance through low mirror roughness," in *2024 International Conference on Optical MEMS and Nanophotonics (OMN)*, 1–2, IEEE (2024). [doi.org/10.1109/OMN61224.2024.10685291].

21 A. Müller, M. C. Wapler, and U. Wallrabe, "A quick and accurate method to determine the Poisson's ratio and the coefficient of thermal expansion of PDMS," *Soft Matter* **15**(4), 779–784 (2019). [doi.org/10.1039/C8SM02105H].

22 M.-A. Bianki, R. Guertin, C. Lemieux-Leduc, *et al.*, "Temperature sensitivity control of an inkjet-printed optical resonator on pillar," *ACS Applied Materials & Interfaces* **16**(4), 5067–5074 (2024). [doi.org/10.1021/acsami.3c14406].

23 S. Timoshenko and S. Woinowsky-Krieger, *Theory of Plates and Shells*, Engineering mechanics series, McGraw-Hill (1959).

24 R. Guertin, M. Pinard, M.-A. Bianki, *et al.*, "Mechanical modeling and optimized design of in-plane Fabry-Perot cavities for polymer swelling sensing," *accepted for publication in the IEEE Journal of Microelectromechanical Systems* (2026). [doi.org/10.1109/JMEMS.2026.3682915].

25 R. Feng and R. J. Farris, "Influence of processing conditions on the thermal and mechanical properties of SU8 negative photoresist coatings," *Journal of Micromechanics and Microengineering* **13**(1), 80 (2002). [doi:10.1088/0960-1317/13/1/312].

26 X. Wu, Y. Wang, Q. Chen, *et al.*, "High-Q, low-mode-volume microsphere-integrated Fabry-

Perot cavity for optofluidic lasing applications," *Photonics Research* **7**(1), 50–60 (2019). [doi.org/10.1364/PRJ.7.000050].

27 A. Muller, E. B. Flagg, J. R. Lawall, *et al.*, "Ultrahigh-finesse, low-mode-volume Fabry-Perot microcavity," *Optics letters* **35**(13), 2293–2295 (2010). [doi.org/10.1364/OL.35.002293].

28 L. Greuter, S. Starosielec, D. Najer, *et al.*, "A small mode volume tunable microcavity: Development and characterization," *Applied Physics Letters* **105**(12) (2014). [doi.org/10.1063/1.4896415].

Régis Guertin is currently pursuing his Ph.D. degree in Engineering Physics in the Microphotonics Laboratory at Polytechnique Montréal. He received his B.Eng. degree and his M.A.Sc. degree in Engineering Physics from Polytechnique Montréal, in 2017 and 2019, respectively. In 2016, he joined Pr. Yves-Alain Peter's laboratory where he has been working on microfabricated optical gas sensors. His research interests include optical resonators, gas detection, and microfabrication of optical components.

Ali Khurshidi is a third-year Engineering Physics student at Polytechnique Montréal and is expected to complete his degree in 2027. In the summer of 2025, he completed an internship in Professor Yves-Alain Peter's laboratory, where he worked on microfabricated gas sensors.

Marc-Antoine Bianki is a current post-doctoral fellow under Prof. Yves-Alain Peter at Polytechnique Montréal. His research expertise lies in optical whispering gallery mode resonators, inkjet printing with polymers, and ultrasonic optical detectors. He completed his B.Eng., M.A.Sc., and Ph.D. in engineering physics at the institution (2018–2025) and is a recipient of the NSERC Postgraduate Scholarship-Doctoral (2019).

Suhas Kottigegollahalli-Sreenivas received his B.E. degree in Electrical and Electronics Engineering from BITS Pilani, Hyderabad Campus, India, in 2025. In 2024, he was a MITACS Globalink Research Intern at Polytechnique Montréal, Montréal, QC, Canada, where he worked in the Microphotonics Laboratory under the supervision of Prof. Yves-Alain Peter on tuning the sensitivity of Fabry–Perot-based optical sensors. His research interests include nanomaterials, microfluidics, nanofabrication, optics, and sensors.

Yves-Alain Peter is currently a professor in the Department of Engineering Physics, Polytechnique Montréal. He received his MSc degree in physics and his DrSc degree from the University of Neuchãtel, Switzerland, in 1994 and 2001, respectively. In 1995, he joined the Department of Medical Radiobiology, Paul Scherrer Institute, Switzerland, as a research associate. From 1995 to 2001, he was a graduate research assistant with the Applied Optics Group, Institute of Microtechnology, University of Neuchãtel. From 2001 to 2003, he was a post-doctoral researcher with the Microphotonics Group, Stanford University. From 2003 to 2004, he was a research and development engineer and a project leader with the Swiss Center for Electronics and Microtechnology, Switzerland. In 2004, he joined Polytechnique Montréal, Canada. His current research interests include microphotonics and micro-opto-electro-mechanical systems.

List of Figures

1 Swelling model of a polymer in a microchannel channel. The dotted line represents the cavity at rest and the dashed line is the swelling without constrains. A) Rigid and B) Flexible mirrors

2 Optical device schematics and location of resonances in red. a) Internal configuration where the optical cavity is located in the polymer's microchannel. b) External configuration where the optical cavity is located outside the polymer's microchannel.

3 1)-4)Fabrication Process. 5) Evaporation setup with evaporation angle β and target metal to evaporate at the source.

4 Optical spectra in external configuration for different cavity length with an empty polymer channel.

5 Wavelength shift as a function of temperature change for two PDMS filled cavities. The reference temperature is $15\,^{\circ}\mathrm{C}$.

6 Normalized temperature sensitivity of SU-8 and PDMS functionalized sensors as a function of the inverse optical cavity length, from $30\,\mu\mathrm{m}$ to $255\,\mu\mathrm{m}$. The mirror thickness of PDMS and SU-8 sensors are $3.7\,\mu\mathrm{m}$ and $2.7\,\mu\mathrm{m}$ respectively. The polymer microchannel is $63\,\mu\mathrm{m}$ long for all devices.

List of Tables